RSC Advances

PAPER

View Article Online
View Journal | View Issue

Cite this: *RSC Adv.*, 2017, **7**, 52604

Effect of Al content on number and location of hydroxyl acid species in zeolites: a DRIFTS quantitative protocol without the need for molar extinction coefficients†

Pierre Bräuer,[a] Pey Ling Ng,[a] Olivia Situmorang,[a] Iain Hitchcock[b] and Carmine D'Agostino *[a]

In this work, we have systematically investigated the effect of the Al content on the number and location of bridging hydroxyls (Brønsted acid sites) and terminal hydroxyls (terminal silanol sites) in ZSM-5 zeolites with varying silica-alumina ratio (SAR = SiO_2/Al_2O_3) using Diffuse Reflectance Infrared Fourier Transform Spectroscopy (DRIFTS) without molar extinction coefficients. Two base probe molecules with different kinetic diameters, pyridine (5.7 Å) and collidine (7.4 Å), were used. The total content of Brønsted acid sites is obtained by elemental analysis of the proton form and sodium exchanged form of ZSM-5. To quantify the number of internal and external Brønsted acid sites the change in area of the Brønsted acid site peak in the O–H stretching region is then used; thus, the need for molar extinction coefficients to quantify Brønsted acid sites is thereby eliminated. The results reported here show that for ZSM-5 the number of external Brønsted sites, in absolute terms, increases with increasing total Al content, as evidenced by collidine adsorption. The number of terminal silanol acid sites was found to be proportional to the external surface area probed by argon sorption experiments. In summary, this work shows that the use of DRIFTS in conjunction with elemental analysis is a valid alternative to qualitatively and quantitatively probe the number and location of hydroxyl acid sites without the use of molar extinction coefficients and gives a comprehensive picture of the effect of Al content on number and location of hydroxyl acid species in ZSM-5 zeolites with varying SAR. The work contributes to advancing the range of characterisation protocols for solid acid catalysts.

Received 27th September 2017
Accepted 4th November 2017

DOI: 10.1039/c7ra10699h

rsc.li/rsc-advances

1. Introduction

Zeolites are crystalline aluminosilicates containing pores and cavities of molecular dimensions. Porous on a molecular scale, zeolites consist of regular arrays of channels and cavities (3–15 Å in diameter) that form a nanoscale labyrinth. Zeolites in their acidic form play an important role in shape-selective heterogeneous catalysis.[1,2] Considerable research has been dedicated towards the characterisation of their surface acidity as the various acid sites on the internal and external zeolite crystal surface are the catalytically active sites in technologically relevant processes such as fluidised catalytic cracking (FCC) to produce gasoline and liquefied petroleum gas (LPG).[3] The number and strength of acid sites in a zeolite is closely linked to its catalytic properties with respect to activity, deactivation rate and product selectivity.[2,4] The location of acid sites is of equal fundamental importance since internal acid sites catalyse size–selective reactions[5–7] and external acid sites catalyse non-size-selective reactions[8–10] or can lead to deactivation of a reaction by coke formation.[11] For example, external acidity is very important in reactions involving molecular species with sizes much larger than the zeolite's typical pore size.[12]

The ZSM-5 zeolite is a medium sized pore zeolite with a three-dimensional channel network containing cavities formed by intersections of straight and zigzag 10-membered rings. The ZSM-5 zeolite structure is widely used as a catalyst in the petrochemical industry due to its unique shape selectivity, surface acidity and thermal stability.[1,13] Therefore, understanding how the aluminium (Al) content in ZSM-5 affects not only the number of catalytically important acid sites but also their location is crucial to understand in order to rationalise, correlate and finally predict their behaviour in solid acid catalysed reactions.

Numerous experimental methods have been developed to study the acidity of zeolites. Microcalorimetry,[14–16] temperature-

[a]*Department of Chemical Engineering and Biotechnology, University of Cambridge, Philippa Fawcett Drive, Cambridge, CB3 0AS, UK. E-mail: cd419@cam.ac.uk; Tel: +44(0)1223-335245*

[b]*Johnson Matthey Technology Centre, Blount's Court, Sonning Common, Reading, RG4 9NH, UK*

† Electronic supplementary information (ESI) available. See DOI: 10.1039/c7ra10699h

programmed desorption (TPD),[17,18] infrared (IR)[19–27] and nuclear magnetic resonance (NMR) spectroscopy[17,28] are among other experimental techniques some of the most frequently used ones. A fundamental challenge of zeolite acidity characterisation is that different experimental techniques provide different aspects of the zeolite acidity, which includes type, number, location and strength of acid sites.

To date, numerous studies have focused on characterising the acidity in ZSM-5 using IR spectroscopy techniques.[19–27] In this regard, an excellent review about the characterisation of surface hydroxyls using IR techniques has been written by Hadjiivanov.[29] However, to the best of our knowledge no study has applied the DRIFTS technique to systematically investigate the effect of Al concentration on the number and location of Brønsted and terminal silanol acid sites exploiting the spectral features in the O–H stretching region. Yet, from the extent of the peak area reduction in the O–H stretching region upon probe molecule adsorption, one can obtain valuable information about the number of acid sites that are accessible to the probe molecule. Furthermore, the shift of such vibrations due to the interaction with probe molecules can provide additional important information, in particular about the strength of the interaction.[21]

Several IR studies[7,30,31] have found that the number of Brønsted acid sites in ZSM-5 increases linearly with increasing total Al content by studying the Brønsted peak in the C=C stretching region using pyridine. It is worth mentioning that the C–C and C–N vibrational modes of pyridine can be used as well to study protonic acidity. Furthermore, other probe molecules used to investigate surface acidity using IR spectroscopy are carbon monoxide (CO), nitrogen (N_2) and ammonia (NH_3) detecting the vibrational modes of C≡O triple bonds, N≡N triple bonds and N–H bonds, respectively. Studies combining IR and solid-state ^{27}Al NMR,[32] TPD[33] or thermal gravimetric analysis (TGA)[16] established the same correlation between the total Al content and the number of Brønsted acid sites.

The number of terminal silanol sites should correlate well with the external surface area,[34] which can be obtained by gas sorption measurements, as terminal silanol hydroxyls are usually located on the external surface of zeolite particles or at framework defects.[2]

Investigating probe molecule accessibility of the ZSM-5 pore network quantitatively is usually conducted by comparing IR peaks that appear in the C=C stretching region. Molar extinction coefficients are then used to quantify the number of probe molecules that can access all acid sites, such as pyridine, and the number of probe molecules that can only access those acid sites located on the external crystal surface or at the pore mouth, such as collidine.

To distinguish the location of acid sites and, hence, the accessibility of probe molecules, different experimental IR procedures have been developed. Thibault-Starzyk *et al.*[35] used an accessibility index (ACI) defined as the ratio of the number of acid sites detected by the probe molecule normalised by the total number of acid sites. In this approach, the total number of acid sites in the zeolite is obtained by measuring the Al content, *e.g.* by elemental analysis. Mlekodaj *et al.*[36] defined an accessibility factor (AF). The AF for collidine interacting with Brønsted sites was defined by the number of collidine molecules adsorbed to Brønsted sites (external surface and pore mouth) divided by the total number probed by pyridine adsorption. These definitions on accessibility have been reported based on the analysis of IR peaks appearing in the C=C stretching region upon probe molecule adsorption. However, to the best of our knowledge, a similar approach based on the change in the IR peak area in O–H stretching region has not been reported yet.

A combination of pyridine and collidine as base probe molecules has been previously used to study the accessibility of acid sites, thus, their location, in ZSM-5.[35–37] IR results[35,36] for ZSM-5 with silica-alumina ratio (SAR) values between 64 and 328 suggested that the total number of Brønsted acid sites accessible to collidine, hence, located at the pore mouth or external ZSM-5 crystal surface, increased with increasing total Al content. However, the data reported in the literature are somehow scarce and fragmentary and do not give a comprehensive picture.

As for terminal hydroxyl sites (terminal silanol sites), several IR studies[20–23,26,27] concluded that these sites are situated on the external ZSM-5 crystal surface independently of the total Al content and crystal size. However, only one study conducted by Armaroli *et al.*[23] investigated this as a function of the SAR (37–137). Other studies did not probe the effect of the Al content in detail.[20–22,26,27]

The objective of this work is to comprehensively study and quantify the effect of the Al content on the number and location of Brønsted acid sites and terminal silanol acid sites in ZSM-5 zeolites with varying SAR using diffuse reflectance IR spectroscopy. Base probe molecules with increasing kinetic diameters, pyridine (5.7 Å) and collidine (7.4 Å), are used to investigate the location dependence of Brønsted and terminal silanol acid sites. Unlike most of previous studies reported on the subject, the aim of this work is to explore the possibility to use changes in IR peak areas in the O–H stretching region to elucidate the location and quantify Brønsted and terminal silanol acid sites. Using this approach, the use of molar extinction coefficients, which are often not available, is not required as there is no need to investigate peaks appearing at lower wavenumbers in the C=C stretching region.

2. Experimental

2.1 Materials and sample preparation

Pyridine (99%) was obtained from Alfa Aesar. Collidine (99%) was obtained from Sigma Aldrich. All chemicals were used as supplied.

Several ZSM-5 samples with various SAR (SiO_2/Al_2O_3) values of 23, 30, 50, 80 and 300 were purchased from Alfa Aesar in the NH_4^+ form. Zeolite samples were calcined in a furnace with synthetic air (100 cm^3 min^{-1}, Air Liquide) at 773 K for 4 h to convert from the NH_4^+ to the H^+ form, termed H-ZSM-5. Heating and cooling were carried out at 5 K min^{-1}. Samples are named according to their SAR, as supplied by Alfa Aesar, and denoted

as H-ZSM-5 (SAR). The surface area of these samples is in the range 400–425 $m^2\ g^{-1}$, as stated by Alfa Aesar.

The sodium (Na^+) form of each SAR of H-ZSM-5 was prepared by exchanging ~2 g of the H^+ form three times for 6 h with 1 M aqueous $NaNO_3$ at 353 K with a magnetic stirrer. At the end of each Na^+ exchange the solution was vacuum-filtered and washed with deionised water three times. After the total of three Na^+ exchange treatments, the filtrate was heated in a furnace with synthetic air (100 $cm^3\ min^{-1}$, Air Liquide) to 393 K at 1 K min^{-1}, held for 2 h, then further heated to 773 K with 2 K min^{-1}, kept there for 4 h and finally cooled to room temperature at 5 K min^{-1}. The IR spectrum of each Na^+ form was examined to confirm the elimination of all Brønsted sites at ~3610 cm^{-1} during the Na^+ exchange procedure.

2.2 Characterisation experiments

To characterise morphological, textural and elemental properties of the H-ZSM-5 zeolite samples, argon sorption, scanning electron microscopy (SEM) and inductively coupled plasma mass spectrometry (ICP-MS) experiments were conducted.

Argon sorption experiments were performed at 87 K by use of a Micromeritics 3Flex apparatus. The sample was placed into a pre-weighed Micromeritics gas sorption tube and a seal frit was placed at the top. A Micromeritics patented isothermal jacket was then placed around the sample tube. The sample tube (with the sample) and the assembly was attached to the ASAP 2020Micromeritics 3Flex and heat treated under vacuum to remove any physisorbed species. The heat treatment involved heating the sample to 363 K under a virtual vacuum (relative pressure 1×10^{-5}) to first remove any physisorbed water. The temperature was then increased to 523 K and the sample was left for 12 hours.

After the heat treatment an argon gas sorption experiment was performed. The gas sorption experiment was fully automated and the relative pressures studied were between 0.004–1.00. At each pressure point the saturation pressure was calculated in a cell, which was adjacent to the sample. At the end of the experiment the sample tube was weighed again to determine the mass of the dried sample.

The specific surface area values were calculated using the Brunauer–Emmett–Teller (BET) equation for argon at 87 K applying the method suggested by Rouquerol *et al.*,[38] where criteria were proposed to extract the specific surface area from a well-defined single linear part of the BET plot. More details can be found elsewhere.[38] The specific external surface area values of H-ZSM-5 zeolites were calculated using thickness layers from an adapted Harkins–Jura equation reported for argon sorption measurements at 87 K in MCM-41 solids[39] to obtain a qualitative trend that could be correlated with the number of external terminal silanol acid sites.[34]

For SEM characterisation, the H-ZSM-5 samples were carbon coated prior to analysis to provide a conductive layer for charge dissipation. The sample powders were dusted directly onto SEM stubs. The samples were then analysed using a Zeiss ultra 55 field emission electron microscope equipped with in-lens secondary electron and backscattered detectors. High-resolution low-accelerating voltage imaging was used. The accelerating voltage was 1.6 kV, the aperture used between 20 and 30 μm and the working distance between 2 to 3 mm. The detectors were in-lens secondary electron and in-lens backscattered electron detectors.

Values for the number-weighted average diameter of H-ZSM-5 crystals were obtained from the agglomerated structures observed in Fig. S3 (see ESI Material†) rather than on individual crystals as a significant better correlation was obtained for the former with the BET surface areas as shown in Fig. S2 (see ESI Material†). For each number-weighted average diameter 20 crystals were counted.

The amount of Al atoms present as framework Al (F-Al) and extra-framework Al (EF-Al) were determined by means of elemental analysis (ICP-MS). Two forms of the zeolite are necessary to perform the calculations. The H^+ form of the zeolite is generated by calcination of the NH_4^+ form of the zeolite as described above. The Na^+ form is generated by Na^+ exchange of the H^+ form with $NaNO_3$ and examination of the O–H stretching region of the IR spectrum to verify complete exchange by the absence of the Brønsted stretching peak (~3610 cm^{-1}) as described above as well. The difference in the Si/Al ratio between the proton and the sodium form is an indicator of how much cationic EF is present in the zeolite. Neutral EF-Al species will not exchange with sodium cations. Furthermore, the Na/Al ratio in the sodium sample should be one or less.

ICP-MS experiments with the proton and sodium form of the ZSM-5 zeolites were performed by Johnson Matthey (Johnson Matthey Technology Centre, Sonning Common). The SARs obtained by elemental analysis were then converted to the total Al concentration per unit cell (Al u.c.) using the chemical formula of ZSM-5 ($H_nAl_nSi_{96-n}O_{192} \times 16H_2O$) giving: Al u.c. = 96/(1 + SAR/2).

2.3 DRIFTS setup and experimental procedure

DRIFTS spectra were recorded on a Nicolet iS50 FT-IR spectrometer (Thermo Scientific) operating at a resolution of 4 cm^{-1} and typically averaging over 128 scans. Spectra were acquired in the region ranging from 400 to 4000 cm^{-1} using a DTGS detector. The high-temperature *in situ* DRIFTS cell with KBr windows was situated in a diffuse reflection accessory (Harrick Scientific Products). A water bath (F6, HAAKE) in conjunction with an electric heater (Series 988, Watlow) was used to control the temperature in the DRIFTS cell. A gas inlet and outlet directed the inert carrier gas stream into the DRIFTS cell and through the KBr or zeolite powder bed. Probe molecules were injected through an injection port, typically 1 μL per injection, until IR peak intensities remained constant.

Background IR spectra for the DRIFTS cell were recorded using KBr powder. For adsorption experiments calcined H-ZSM-5 powder (~20 mg) without further preparation was placed in the DRIFTS cell, no compression was applied, and supported on quartz wool resulting in a sample thickness of ~3 mm. The reproducibility of the DRIFTS results and the effect of particle size, packing density and sample thickness is discussed in more detail in the ESI Material† (Paragraph S.4.).

Typically, the zeolite sample was heated to 673 K at 5 K min^{-1} in flowing helium (100 cm^3 min^{-1}, Air Liquide), held for 1 hour, and then cooled to 300 K at 5 K min^{-1}. Probe molecules were injected into the cell *via* the injection port using a 10 μL syringe (Hamilton) until IR peak intensities did not change anymore and IR spectra were then acquired.

The different amounts of sample powder used in each DRIFTS experiment and, therefore, the number of surface hydroxyls detectable by IR spectroscopy must be accounted for if the DRIFTS spectra should be compared quantitatively. To normalise the DRIFTS spectra the overtone and combination vibrations found between 1750 and 2100 cm^{-1} in the activated spectrum can be used as an internal standard. Hence, all integrated peak intensities (I_{peak}) were normalised by the area of the overtone and combination vibrations found between 1750 and 2100 cm^{-1} ($I_{1750-2100}$) as follows:[7,40]

$$I_{peak,normalised} = \frac{I_{peak}}{I_{1750-2100}} \quad (1)$$

Using eqn (1), the peak intensities for surface hydroxyl groups, such as Brønsted and terminal silanol groups in the O–H stretching region, can be quantitatively compared. In addition to quantitatively interpret the IR spectroscopy results the selection of the appropriate conversion function, absorbance or Kubelka–Munk (KM), for DRIFTS spectra was investigated. The results can be found in the ESI Material† (Paragraph S.4.). From this analysis, the absorbance function was chosen.

3. Results and discussion

3.1 Zeolite characterisation results

The H-ZSM-5 zeolite samples with varying SAR were characterised by argon sorption isotherms, SEM experiments and elemental analysis of the proton (H^+) and sodium (Na^+) forms of the ZSM-5 zeolites, respectively.

The argon sorption isotherms in H-ZSM-5 are depicted on a linear scale in Fig. 1 (left) and on a logarithmic scale in Fig. 1 (right), respectively. All five investigated samples showed a combination of isotherms of type I and IV. The micropores are filled up at low relative pressures ($p/p_0 \approx 0.1$). At $p/p_0 \approx 0.9$ a progressive argon uptake appears and for lower relative pressures the corresponding hysteresis loop can be observed, which implies the existence of irregular mesoporous structures. The hysteresis loop closes at $p/p_0 \approx 0.4$ for all SARs of H-ZSM-5 except 300 for which the loop closes at $p/p_0 \approx 0.5$. It is clear from Fig. 1 (left) that the BET surface area is different for the various SARs. However, no trend is observed with the total Al content (see Fig. S1 in ESI Material†). By inspection of Fig. 1 (right) it can be seen that the micropore region ($p/p_0 < 10^{-3}$) shows no significant differences among the samples studied. An additional step can be observed at $p/p_0 \approx 10^{-3}$, which is frequently explained by a fluid-to-crystalline like phase transition[41,42] and is not indicative of any real porosity.

From the argon sorption isotherms, the specific surface area was calculated using the BET method suggested by Rouquerol *et al.*[38] to extract meaningful BET surface area values. The results are reported in Table 1. The values are typical for H-ZSM-5 zeolites and agree well with values reported elsewhere.[43,44] It can be observed in Table 1 that the measured BET surface area values for the H^+ form of ZSM-5 are 10 to 20% higher relative to the surface values supplied by Alfa Aesar for the NH_4^+ form of ZSM-5.

Furthermore, specific external surface areas were extracted from the argon sorption measurements using a Harkins–Jura equation reported elsewhere.[45] The results show that there is a maximum for the specific external surface area for H-ZSM-5 (50). Values for the average diameter of H-ZSM-5 crystals were obtained from SEM characterisation experiments and are listed in Table 1 as well. The range of values is very narrow especially for SARs between 50 and 300. A clear Al content trend, as has been reported in some cases,[46] is not observed here (see Fig. S1 in ESI Material†).

The SEM characterisation and elemental analysis results are discussed in the ESI Material† in Paragraph S.2 and S.3, respectively.

3.2 Effect of Al content on number of acid sites in H-ZSM-5

Typical activated IR spectra of the five investigated H-ZSM-5 zeolite samples in the O–H stretching region are shown Fig. 2. As described in the experimental section, the spectra were normalised using the areas of the overtone and combination vibrations between 1750 and 2100 cm^{-1} to account for the different amounts of H-ZSM-5 powder used in each experiment. Thus, the IR spectra can quantitatively be compared.

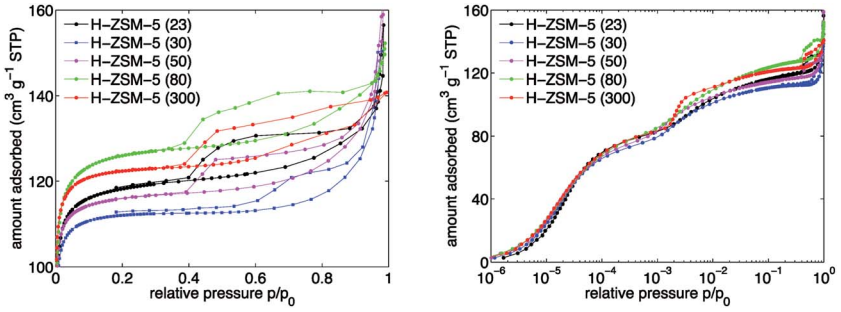

Fig. 1 Argon sorption isotherms in H-ZSM-5 with varying SAR from 23 to 300 over relative pressure (p/p_0) for (left) normal scale and (right) log scale. The *y*-scale on the left figure is zoomed in to 100 to 160 cm^3 g^{-1} STP.

Table 1 Surface area supplied from Alfa Aesar for the NH_4^+ form of ZSM-5 and BET area and external surface area extracted from argon sorption isotherms in H-ZSM-5 zeolites with varying SAR and their respective crystal size obtained by SEM characterisation

SAR[a]	Surface area[a] ($m^2\ g^{-1}$)	BET area[b] ($m^2\ g^{-1}$)	$Area_{external}$[c] ($m^2\ g^{-1}$)	$d_{crystal}$[d] (μm)
23	425	467	45	2.7 ± 1.3
30	400	449	60	4.1 ± 1.6
50	425	463	63	1.8 ± 0.6
80	425	497	59	1.2 ± 0.3
300	400	484	33	1.8 ± 0.4

[a] As supplied by Alfa Aesar for the NH_4^+ form of ZSM-5. [b] Extracted from argon sorption experiments, error estimated to 2%. [c] Calculated using the Harkins–Jura equation for argon at 87 K reported by Kruk and Jaroniec,[45] error estimated to 5%. [d] Obtained from SEM characterisation.

The peak at ~3610 cm^{-1}, associated with Brønsted acid sites, is the most pronounced for H-ZSM-5 (23) and decreases with increasing SAR, hence, decreasing Al content. The dependence of the peak at ~3740 cm^{-1}, assigned to terminal silanol acid sites, is more difficult to visualise. In more detail, the peak area does not seem to vary significantly between H-ZSM-5 (23) and H-ZSM-5 (80). However, the peak is clearly reduced for H-ZSM-5 (300).

For H-ZSM-5 (30) and H-ZSM-5 (50) bands at ~3660 and ~3777 cm^{-1} can also be identified, the former being more strongly pronounced, which are normally assigned to the presence of EF-Al located at the internal surface.[22,47]

The spectra of H-ZSM-5 (50) to (300) evidence a broad band around 3500 cm^{-1} indicating the presence of internal silanol sites at framework defects, frequently referred to as "nests".[48,49] However, some studies have suggested that the broad band between 3200 and 3600 cm^{-1} can be assigned to a combination of both internal silanol sites at framework defects (nests) and distorted bridging hydroxyl species, that is, Brønsted acid sites interacting with framework oxygen atoms.[50–53]

The variation of the activated Brønsted peak area (~3610 cm^{-1}), which relates to the number of sites, with the total Al concentration is depicted in Fig. 3. The area of the Brønsted acid site peak is approximately proportional to the total Al content in H-ZSM-5. The results presented in Fig. 3 suggest that H-ZSM-5 (23) has the highest number of Brønsted acid sites. Increasing the SAR, and hence decreasing the total Al content, the number of Brønsted acid sites decreases. The observed trend is in good agreement with previous results[7,30,31] and suggests that the experimental DRIFTS setup designed to probe the number of acid sites on the internal and external surface of H-ZSM-5 provides quantitative results.

Terminal silanol hydroxyls (~3740 cm^{-1}) are located on the external surface of zeolite particles or at framework defects.[2] In this regard, it has been suggested that the number of those sites depends on the external surface area of a zeolite,[34] although a definitive conclusion has not yet been reached. The external surface area can be obtained by gas sorption experiments. In this work, argon sorption experiments were used to characterise the H-ZSM-5 samples and to extract the external surface area values using the Harkins–Jura equation adopted to argon sorption data in MCM-41 materials.[45] The correlation of the terminal silanol peak areas against the values of the external surface area of H-ZSM-5 is depicted in Fig. 4. It can be observed that a good agreement is obtained between the two. Hence, the results reported here confirm those earlier findings[34] and strengthen the idea that terminal silanol sites are closely linked to external surface area of the zeolite particles.

A dependence of the number of terminal silanol sites with H-ZSM-5 crystal size as suggested based on the IR results reported by Armaroli *et al.*[23] is not observed for the H-ZSM-5 samples investigated in this study as verified by SEM characterisation results reported in Table 1. The discrepancy related to the crystal size can be explained by the SEM results (see Fig. S3 in

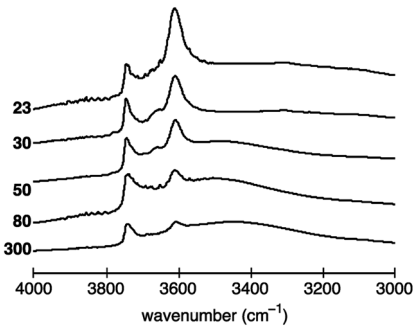

Fig. 2 Normalised activated IR spectra of H-ZSM-5 with a SAR of 23, 30, 50, 80 and 300 between 3000 to 4000 cm^{-1}. The vertical axis (absorbance) has arbitrary units.

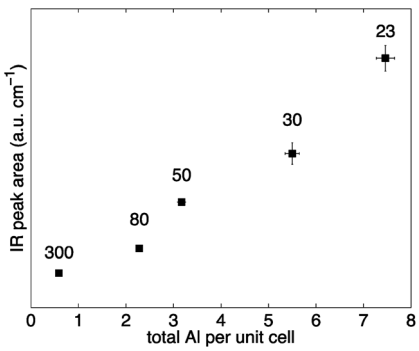

Fig. 3 Normalised areas of activated Brønsted IR peak (~3610 cm^{-1}) over the total Al concentration per unit cell for H-ZSM-5 with different SAR (300, 80, 50, 30 and 23 from left to right). Error bars were calculated from the standard deviation of three separate IR experiments (*y*-values) and from the uncertainty involved in the elemental analysis experiments (*x*-values). Values for the mean and standard deviation can be found in Table S2 in the ESI Material.†

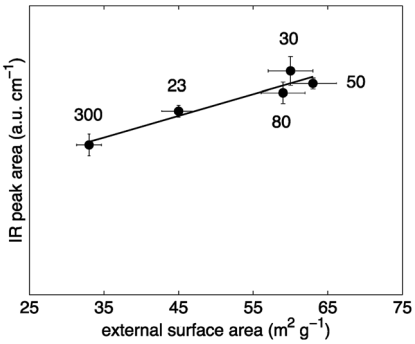

Fig. 4 Normalised areas of activated silanol IR peak (~3740 cm^{-1}) over external surface area of H-ZSM-5 with different SAR (indicated in the plot). The external surface area values were extracted from argon sorption measurements. Error bars of terminal silanol peak areas were calculated from the standard deviation of three separate IR experiments (*y*-values) and estimated with 5% for the surface area values (*x*-values).

ESI Material†). The investigated H-ZSM-5 zeolites consist of agglomerates of fine particles. In contrast to the other four H-ZSM-5 samples, H-ZSM-5 (300) has approximately spherical structures that did not seem to be agglomerated. Hence, due to the agglomeration the average crystal diameter of the studied H-ZSM-5 samples, obtained by SEM, is not likely to correlate with the external surface area, obtained by argon sorption, and, therefore, not with the number of terminal silanol acid sites. The possible difference between the external surface area measured by gas sorption and the calculated surface area based on the crystal diameter has already been reported elsewhere.[54]

Synthesis conditions can greatly affect the final zeolite acidity properties.[55–58] Thus, a direct comparison between different studies is often difficult. However, the results reported in Fig. 4 suggest that the number of terminal silanol sites depends on the external surface area obtained by gas sorption measurements. Interestingly, the external surface area of the studied H-ZSM-5 zeolites is not proportional to the zeolite crystal size or the external surface area calculated based on the diameter of the zeolite crystal as verified from the values reported in Table 1 obtained by SEM characterisation. Hence, it is crucial to characterise zeolites using gas sorption measurements when the number of external terminal silanol sites is of importance such as in non-shape selective reactions.[8–10]

3.3 Effect of Al content on location of acid sites in H-ZSM-5

To study the location dependence of both Brønsted and terminal silanol acid sites on the Al content in H-ZSM-5, IR experiments were conducted with base probe molecules exhibiting different kinetic diameters. Pyridine with a kinetic diameter of ~5.7 Å is able to access all acid sites present on the internal and external H-ZSM-5 surface.[35] However, the bulkier probe molecule collidine, having a kinetic diameter of ~7.4 Å, is not able to access the acid sites located in the H-ZSM-5 pore network but only those located on the external H-ZSM-5 crystal surface and the entrances of the pore network, termed pore mouth.[26,35,36]

The normalised IR spectra for all five H-ZSM-5 samples prior to probe molecule adsorption and after probe molecule adsorption for either (a) pyridine or (b) collidine are shown in Fig. 5.

Depicted are the Brønsted acid peak (~3610 cm^{-1}) and the peak assigned to terminal silanol sites (~3740 cm^{-1}). The solid line represents the IR spectrum prior to probe molecule adsorption. The filled circles show the IR spectrum after probe molecule adsorption for either (a) pyridine or (b) collidine. The different spectra are discussed in the following to determine the location of Brønsted and terminal silanol acid sites and their distribution between the internal and external surface, if applicable.

Firstly, it can be observed in Fig. 5 that for H-ZSM-5 (30) and H-ZSM-5 (50) the IR band at 3660 cm^{-1} assigned to hydroxyls associated with EF-Al species located at the internal surface completely disappears after pyridine adsorption but does hardly change after collidine adsorption confirming that those hydroxyls are mainly located inside the zeolite pore network as suggested elsewhere.[22,47]

Furthermore, Fig. 5 shows that the Brønsted peak (~3610 cm^{-1}) disappears for all five H-ZSM-5 samples investigated once pyridine, plots (a), is adsorbed. Hence, the IR spectra clearly suggest that pyridine molecules can interact with all Brønsted acid sites present on the H-ZSM-5 surface, regardless of the Al content. Indeed, even though the kinetic diameter of pyridine is comparable to the pore dimensions of H-ZSM-5, pyridine is expected to enter the H-ZSM-5 pore network, evidenced by having an ACI of near unity reported elsewhere.[59]

When collidine, plots (b) in Fig. 5, is adsorbed the Brønsted peak is only slightly perturbed. The extent to which the Brønsted peak is reduced upon collidine exposure differs for the five H-ZSM-5 samples investigated. Collidine has a kinetic diameter of 7.4 Å, which is larger than the pore size of H-ZSM-5 (sinusoidal channels: 5.3 Å × 5.6 Å, straight channels: 5.5 Å × 5.1 Å)[13] and is thus not expected to enter the pore network. However, the reduced Brønsted peak observed for all SARs studied suggests that collidine molecules can interact with Brønsted acid sites, which are possibly located at the pore mouth or at the external H-ZSM-5 crystal surface.[60] However, the Brønsted acid sites accessible to collidine are more likely to be located at the pore mouth than the external crystal surface.[35]

It is important to point out that it has been reported that strong bases such as pyridine strongly attract surface protons, thus, can induce a change in location compared to their initial location.[61,62] In this regard, the pyridine results illustrated in Fig. 5 are not likely to be significantly affected by such change in proton location. Nonetheless, the stronger base collidine could theoretically attract protons located further inside the channels that would not be accessible to collidine when only considering the difference in size, that is, the kinetic diameter of collidine and the H-ZSM-5 pore network.

The fraction of Brønsted sites that collidine can access varies with the total Al content. To further investigate this, the peak areas for the IR spectra prior to probe molecule adsorption and after probe molecule adsorption were determined and normalised by the area of the overtone and combination vibrations

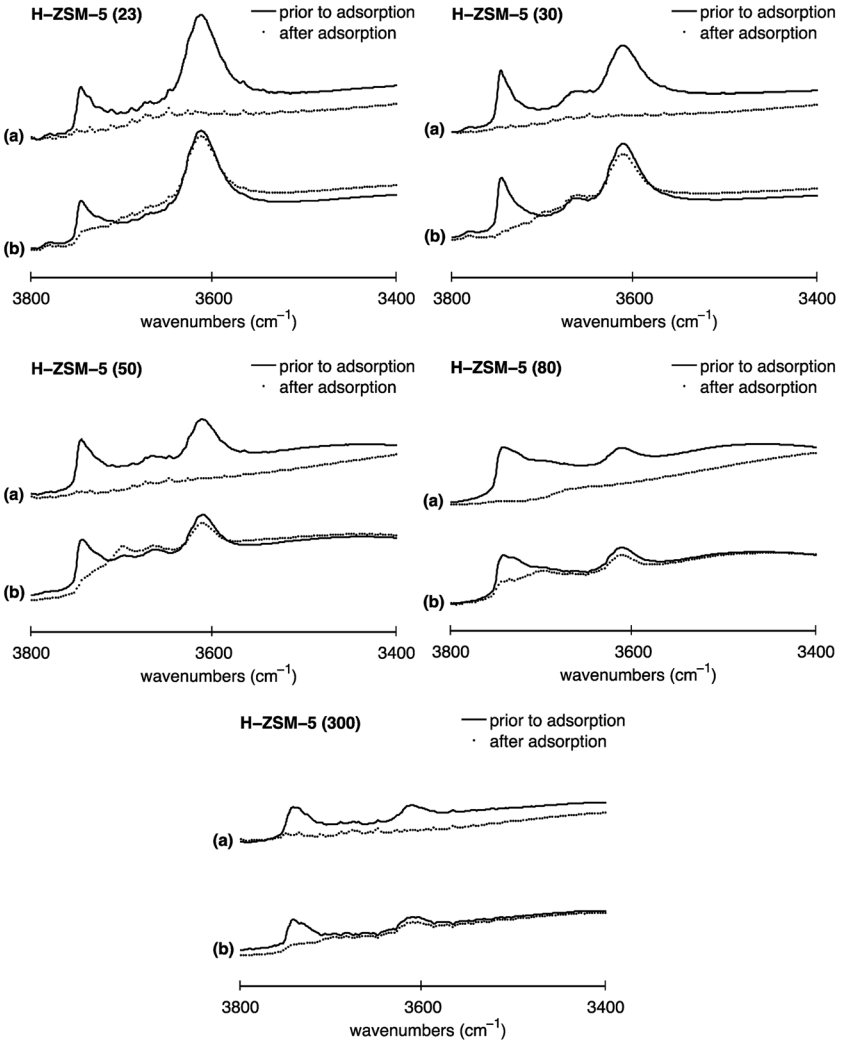

Fig. 5 Normalised IR spectra of H-ZSM-5 with SAR values of 23, 30, 50, 80 and 300 for (a) pyridine and (b) collidine adsorption in the O–H stretching region (3400 to 3800 cm^{-1}): (solid line) spectrum prior to probe molecule adsorption, (filled circles) spectrum after probe molecule adsorption. The *y*-axis (absorbance a.u.) in each plot has the same scale hence spectra can directly be compared. IR spectra after probe molecule adsorption in the O–H stretching region (3000 to 4000 cm^{-1}) can be found in Fig. S6 in the ESI Material.†

between 1750 and 2100 cm^{-1}. Then, the area reduction, area (Δ), given by:

$$\text{Area } (\Delta) = (\text{area}_{\text{prior}} - \text{area}_{\text{after}}) \quad (2)$$

was calculated. In eqn (2) the symbol $\text{area}_{\text{prior}}$ represents the area of the IR peak prior to probe molecule adsorption, hence, without adsorbed moisture. Further, $\text{area}_{\text{after}}$ stands for the area of the IR peak after probe molecule adsorption on the H-ZSM-5 surface, in this case collidine.

Thus, the area reduction is proportional to the number of acid sites that the probe molecule is adsorbed on. The results are shown in Fig. 6. Depicted are the Brønsted areas prior to collidine adsorption (filled squares) and the Brønsted areas after collidine adsorption (empty squares). Additionally, the difference between the two areas, that is, the area reduction (Δ) defined in eqn (2), is shown (filled circles). External Brønsted acid sites are defined as those accessible to collidine molecules, which are proportional to the area reduction (Δ). Conversely, internal Brønsted acid sites are proportional to the Brønsted peak area that was not reduced upon collidine adsorption, that is, the area after collidine adsorption.

It can be observed in Fig. 6 that the Brønsted peak area prior to adsorption is reduced by collidine adsorption indicating that external Brønsted acid sites are present in the investigated H-ZSM-5 samples regardless of the framework Al content. The trend of the number of external Brønsted acid sites with the framework Al content is more straightforward to see when plotted as the area reduction (Δ) as this represents the area that was reduced due to collidine adsorption. Fig. 6 shows that the number of external Brønsted acid sites increases with increasing framework Al content in H-ZSM-5 (filled circles). Therefore, the collidine IR results suggest that H-ZSM-5 (300), lowest Al content, has the lowest number of external Brønsted acid site and H-ZSM-5 (23), highest Al content, has the highest number, although very comparable to H-ZSM-5 (30).

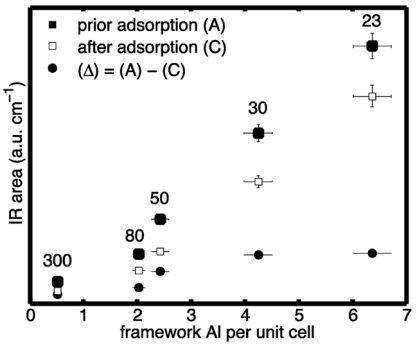

Fig. 6 Normalised areas of: (filled squares) Brønsted peak prior to collidine adsorption; (empty squares) Brønsted peak after collidine adsorption; and (filled circles) difference between the two, that is, the area reduction (Δ), over the framework Al concentration per unit cell for H-ZSM-5 with different SAR (300, 80, 50, 30 and 23 from left to right). Values for the mean and standard deviation can be found in Table S3 in the ESI Material.†

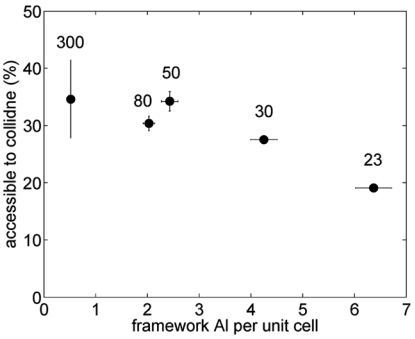

Fig. 7 Percentage of Brønsted peak area accessible to collidine probe molecules over the framework Al concentration per unit cell for H-ZSM-5 with different SAR (300, 80, 50, 30 and 23 from left to right). Error bars for the y-values were estimated from integration limit variation and multiple IR spectra analysis. Values for the mean and standard deviation can be found in Table S4 in the ESI Material.†

Interestingly, even though H-ZSM-5 (23) has significantly more internal Brønsted sites than H-ZSM-5 (30), their number of external Brønsted sites is equal within the experimental uncertainty.

The fraction of collidine molecules that can interact with Brønsted acid sites was calculated by dividing the area reduction, defined in (2), of the Brønsted peak due to collidine adsorption, $\text{area}_{\text{Brønsted}}$ (Δ), by the number of Brønsted sites available in the first place, that is, the Brønsted area prior to collidine adsorption, $\text{area}_{\text{Brønsted,prior}}$, as follows:

$$\text{Accessible to collidine}(\%) = \frac{\text{area}_{\text{Brønsted}}(\Delta)}{\text{area}_{\text{Brønsted,prior}}} \times 100 \qquad (3)$$

The results of this analysis are illustrated in Fig. 7. Interestingly, the fraction of external Brønsted sites decreases with increasing framework Al content. The observed decreasing trend with increasing framework Al content is not that surprising as the number of external Brønsted sites does not vary much with framework Al content but the number of Brønsted acid sites located inside the channels does significantly increase with higher framework Al content. Hence, the percentage of the overall Brønsted sites that are accessible to collidine molecules is low at higher framework Al content as most Brønsted acid sites are located inside the pore network. For low framework Al content the percentage of Brønsted sites accessible to collidine molecules is much higher as the number of Brønsted sites located inside the channels is much lower compared to higher Al concentrations.

The data reported in the literature concerning the distribution of Brønsted acid sites[35,36] are somehow scarce and fragmentary. One IR study[36] investigated ZSM-5 with two SARs of 32 and 164 and found that the total number of Brønsted acid sites accessible to collidine increased with increasing total Al content. Further, it was reported that the AF of collidine, *i.e.*, number of Brønsted sites probed by collidine (external/pore mouth) divided by number of Brønsted sites probed by pyridine (total), decreased with increasing total Al content.

Here we systematically study the distribution of Brønsted acid sites over a much wider range of Al concentrations, which provides a more comprehensive picture on which we are able to draw more robust conclusions.

Additionally, it has been reported that the ACI of ZSM-5 samples, obtained using pyridine and 2,6-dimethylpyridine (DMPy), correlated with the external surface area probed by N_2 sorption experiments.[60] In more detail, the ACI was found to increase with increasing external surface area. In this regard, the percentage of Brønsted acid sites accessible to collidine is somewhat comparably defined as the ACI. Comparing the results depicted in Fig. 7 with the external surface area values reported in Table 1 it can be observed that no correlation between the two parameters exists in this work.

We now analyse in more detail the distribution of terminal silanol sites. Upon pyridine adsorption, the IR peak assigned to terminal silanol sites ($\sim$3740 cm^{-1}) completely disappeared for all five H-ZSM-5 samples, which can be seen in Fig. 5, plots (a). Hence, the results suggest that pyridine can access all terminal silanol sites present on the H-ZSM-5 surface independently of the Al content. However, pyridine probes internal and external acid sites so no conclusion about their location can be drawn from this. Using collidine in conjunction with pyridine the presence of terminal silanol sites on either the internal surface, external surface or both surfaces can be probed. IR collidine adsorption results depicted in Fig. 5, plots (b), show that the peak at $\sim$3740 cm^{-1}, assigned to terminal silanol sites, is strongly reduced for all five H-ZSM-5 samples. For H-ZSM-5 (30) the terminal silanol peak completely disappeared. Given that collidine does not access the internal acid sites, we conclude that most terminal silanol acid sites are located on the external H-ZSM-5 crystal surface or at the pore mouth regardless of the Al content. Hence, the results indicate that only a small fraction of terminal silanol acid sites are located in the pore network. The results agree with earlier studies[20–23,26,27] and, in addition, suggest that this is the case for a wide range of SAR.

4. Conclusions

The aim of this work was to study, using a quantitative approach, the effects of the Al content on the number and location of Brønsted and terminal silanol acid sites in H-ZSM-5 zeolites with varying SARs. Two base probe molecules with different kinetic diameter in conjunction with diffusive reflectance IR experiments were used to elucidate the H-ZSM-5 acidity properties. Pyridine (5.7 Å) was used to investigate all acid sites present on the H-ZSM-5 zeolite surface. Collidine, with a kinetic diameter of 7.4 Å, was used to probe acid sites located at the pore mouth or external H-ZSM-5 zeolite surface. Compared to the frequent applied method of determining the Brønsted IR intensities at lower wavenumbers upon adsorption of basic probe molecules and using molar extinction coefficients to obtain the number of probe molecules adsorbed to Brønsted acid sites, this work explored a different experimental method in which molar extinction coefficients are not needed. The total Brønsted acid site concentration was determined by elemental analysis of the proton (H^+) form and the sodium (Na^+) exchanged form of ZSM-5. The possibility of using the change of IR intensities of the Brønsted acid site peak in the O–H stretching region to study the location was then explored. The number of terminal silanol acid sites and their location was also investigated quantitatively using the IR intensity in the O–H stretching region probed by DRIFTS. In summary:

- The results indicate that the total number of Brønsted acid sites increases with total Al concentration, hence, decreasing SAR.
- The number of terminal silanol sites was found to be proportional to the external surface area of the zeolite as probed by argon adsorption.
- In terms of acid site location, the total number of external Brønsted sites increased with increasing framework Al content as evidenced by collidine adsorption, whereas the fraction of these external Brønsted sites, probed by collidine, relative to the total number of Brønsted sites, probed by pyridine, decreased with increasing framework Al content.
- Terminal silanol sites were found to be mostly located on the external H-ZSM-5 crystal surface.

This work has shown that diffuse reflectance IR spectroscopy can be used for the quantitative study of surface hydroxyls, Brønsted and terminal silanol acid sites, by probing the change in IR intensities in the O–H stretching region, using differently sized base probe molecules, pyridine and collidine. This new approach allowed us to obtain quantitative information on number and location of hydroxyl species in H-ZSM-5 with varying Al content without the need of molar extinction coefficients.

Conflicts of interest

There are no conflicts to declare.

Acknowledgements

Carmine D'Agostino is grateful to Wolfson College, Cambridge, for supporting his research activities. We would also like to acknowledge Prof. Lynn Gladden from the University of Cambridge and Dr Andy York from Johnson Matthey.

References

1 *Zeolites in industrial separation and catalysis*, ed. S. Kulprathipanja, Wiley-VCH, Weinheim, 2010.
2 *Zeolites and catalysis: synthesis, reactions and applications*, ed. J. Čejka, A. Corma and S. Zones, Wiley-VCH, Weinheim, 2010.
3 C. S. Cundy and P. A. Cox, *Chem. Rev.*, 2003, **103**, 663–702.
4 E. G. Derouane, J. C. Védrine, R. R. Pinto, P. M. Borges, L. Costa, M. A. N. D. A. Lemos, F. Lemos and F. R. Ribeiro, *Catal. Rev.*, 2013, **55**, 454–515.
5 E. G. Derouane, J.-M. Andre and A. A. Lucas, *J. Catal.*, 1988, **110**, 58–73.
6 R. Gounder and E. Iglesia, *J. Am. Chem. Soc.*, 2009, **131**, 1958–1971.
7 A. Janda and A. T. Bell, *J. Am. Chem. Soc.*, 2013, **135**, 19193–19207.
8 G. Paparatto, E. Moretti, G. Leofanti and F. Gatti, *J. Catal.*, 1987, **105**, 227–232.
9 S. Melson and F. Schüth, *J. Catal.*, 1997, **170**, 46–53.
10 T. Kunieda, J.-H. Kim and M. Niwa, *J. Catal.*, 1999, **188**, 431–433.
11 M. Bjørgen, S. Svelle, F. Joensen, J. Nerlov, S. Kolboe, F. Bonino, L. Palumbo, S. Bordiga and U. Olsbye, *J. Catal.*, 2007, **249**, 195–207.
12 S. Xing, P. Lv, J. Wang, J. Fu, P. Fan, L. Yang, G. Yang, Z. Yuan and Y. Chen, *Phys. Chem. Chem. Phys.*, 2017, **19**, 2961–2973.
13 H. van Koningsveld, *Compendium of zeolite framework types: building schemes and type characteristics*, Elsevier, Amsterdam; London, 1st edn, 2007.
14 A. Auroux, V. Bolis, P. Wierzchowski, P. C. Gravelle and J. C. Vedrine, *J. Chem. Soc., Faraday Trans. 1*, 1979, **75**, 2544–2555.
15 D. T. Chen, S. B. Sharma, I. Filimonov and J. A. Dumesic, *Catal. Lett.*, 1992, **12**, 201–211.
16 Y.-H. Yeh, R. J. Gorte, S. Rangarajan and M. Mavrikakis, *J. Phys. Chem. C*, 2016, **120**, 12132–12138.
17 L. Rodríguez-González, F. Hermes, M. Bertmer, E. Rodríguez-Castellón, A. Jiménez-López and U. Simon, *Appl. Catal., A*, 2007, **328**, 174–182.
18 F. Jin and Y. Li, *Catal. Today*, 2009, **145**, 101–107.
19 M. Trombetta, G. Busca, S. Rossini, V. Piccoli, U. Cornaro, A. Guercio, R. Catani and R. J. Willey, *J. Catal.*, 1998, **179**, 581–596.
20 T. Armaroli, M. Trombetta, A. G. Alejandre, J. R. Solis and G. Busca, *Phys. Chem. Chem. Phys.*, 2000, **2**, 3341–3348.
21 M. Trombetta, T. Armaroli, A. Gutièrrez Alejandre, J. Ramirez Solis and G. Busca, *Appl. Catal., A*, 2000, **192**, 125–136.
22 T. Armaroli, M. Bevilacqua, M. Trombetta, F. Milella, A. G. Alejandre, J. Ramírez, B. Notari, R. J. Willey and G. Busca, *Appl. Catal., A*, 2001, **216**, 59–71.
23 T. Armaroli, L. J. Simon, M. Digne, T. Montanari, M. Bevilacqua, V. Valtchev, J. Patarin and G. Busca, *Appl. Catal., A*, 2006, **306**, 78–84.

24 T. Montanari, M. Bevilacqua and G. Busca, *Appl. Catal., A*, 2006, **307**, 21–29.
25 K. Suzuki, T. Noda, N. Katada and M. Niwa, *J. Catal.*, 2007, **250**, 151–160.
26 M. S. Holm, S. Svelle, F. Joensen, P. Beato, C. H. Christensen, S. Bordiga and M. Bjørgen, *Appl. Catal., A*, 2009, **356**, 23–30.
27 D. Tzoulaki, A. Jentys, J. Pérez-Ramírez, K. Egeblad and J. A. Lercher, *Catal. Today*, 2012, **198**, 3–11.
28 W. Zhang, D. Ma, X. Liu, X. Liu and X. Bao, *Chem. Commun.*, 1999, 1091–1092.
29 K. Hadjiivanov, in *Advances in Catalysis*, ed. F. C. Jentoft, Academic Press, 2014, vol. 57, pp. 99–318.
30 N.-Y. Topsøe, K. Pedersen and E. G. Derouane, *J. Catal.*, 1981, **70**, 41–52.
31 N. Brodu, M.-H. Manero, C. Andriantsiferana, J.-S. Pic and H. Valdés, *Chem. Eng. J.*, 2013, **231**, 281–286.
32 P. Sazama, B. Wichterlova, J. Dedecek, Z. Tvaruzkova, Z. Musilova, L. Palumbo, S. Sklenak and O. Gonsiorova, *Microporous Mesoporous Mater.*, 2011, **143**, 87–96.
33 A. S. Al-Dughaither and H. de Lasa, *Ind. Eng. Chem. Res.*, 2014, **53**, 15303–15316.
34 S.-B. Pu and T. Inui, *Zeolites*, 1997, **19**, 452–454.
35 F. Thibault-Starzyk, I. Stan, S. Abelló, A. Bonilla, K. Thomas, C. Fernandez, J.-P. Gilson and J. Pérez-Ramírez, *J. Catal.*, 2009, **264**, 11–14.
36 K. Mlekodaj, K. Tarach, J. Datka, K. Góra-Marek and W. Makowski, *Microporous Mesoporous Mater.*, 2014, **183**, 54–61.
37 B.-T. L. Bleken, L. Mino, F. Giordanino, P. Beato, S. Svelle, K. P. Lillerud and S. Bordiga, *Phys. Chem. Chem. Phys.*, 2013, **15**, 13363–13370.
38 J. Rouquerol, P. Llewellyn and F. Rouquerol, *Stud. Surf. Sci. Catal.*, 2007, **160**, 49–56.
39 M. Kruk and M. Jaroniec, *Microporous Mesoporous Mater.*, 2001, **44**, 725–732.
40 S. M. Maier, A. Jentys and J. A. Lercher, *J. Phys. Chem. C*, 2011, **115**, 8005–8013.
41 W. S. Borghard, P. T. Reischman and E. W. Sheppard, *J. Catal.*, 1993, **139**, 19–23.
42 J. C. Groen, L. A. A. Peffer and J. Pérez-Ramírez, *Microporous Mesoporous Mater.*, 2003, **60**, 1–17.
43 J. Lu, Z. Zhao, C. Xu, A. Duan, X. Wang and P. Zhang, *J. Porous Mater.*, 2007, **15**, 213–220.
44 M. Milina, S. Mitchell, N.-L. Michels, J. Kenvin and J. Pérez-Ramírez, *J. Catal.*, 2013, **308**, 398–407.
45 M. Kruk and M. Jaroniec, *Chem. Mater.*, 2000, **12**, 222–230.
46 L. Shirazi, E. Jamshidi and M. R. Ghasemi, *Cryst. Res. Technol.*, 2008, **43**, 1300–1306.
47 V. V. Ordomsky, V. Y. Murzin, Y. V. Monakhova, Y. V. Zubavichus, E. E. Knyazeva, N. S. Nesterenko and I. I. Ivanova, *Microporous Mesoporous Mater.*, 2007, **105**, 101–110.
48 R. M. Dessau, K. D. Schmitt, G. T. Kerr, G. L. Woolery and L. B. Alemany, *J. Catal.*, 1987, **104**, 484–489.
49 R. M. Dessau, K. D. Schmitt, G. T. Kerr, G. L. Woolery and L. B. Alemany, *J. Catal.*, 1988, **109**, 472–473.
50 E. Bourgeat-Lami, P. Massiani, F. Di Renzo, P. Espiau, F. Fajula and T. Des Courières, *Appl. Catal.*, 1991, **72**, 139–152.
51 I. Kiricsi, C. Flego, G. Pazzuconi, W. O. J. Parker, R. Millini, C. Perego and G. Bellussi, *J. Phys. Chem.*, 1994, **98**, 4627–4634.
52 I. Papai, A. Goursot, F. Fajula and J. Weber, *J. Phys. Chem.*, 1994, **98**, 4654–4659.
53 S. Bordiga, B. Civalleri, G. Spoto, C. Pazè, C. Lamberti, P. Ugliengo and A. Zecchina, *J. Chem. Soc., Faraday Trans.*, 1997, **93**, 3893–3898.
54 S. Melson and F. Schüth, *J. Catal.*, 1997, **170**, 46–53.
55 C. J. H. Jacobsen, C. Madsen, T. V. W. Janssens, H. J. Jakobsen and J. Skibsted, *Microporous Mesoporous Mater.*, 2000, **39**, 393–401.
56 J. Čejka and B. Wichterlová, *Catal. Rev.*, 2002, **44**, 375–421.
57 R. Barakov, N. Shcherban, P. Yaremov, V. Solomakha, A. Vyshnevskyy and V. Ilyin, *J. Porous Mater.*, 2015, 1–12.
58 J. Li, S. Liu, H. Zhang, E. Lü, P. Ren and J. Ren, *Chin. J. Catal.*, 2016, **37**, 308–315.
59 D. Verboekend and J. Pérez-Ramírez, *Catal. Sci. Technol.*, 2011, **1**, 879–890.
60 Z. Xue, T. Zhang, J. Ma, H. Miao, W. Fan, Y. Zhang and R. Li, *Microporous Mesoporous Mater.*, 2012, **151**, 271–276.
61 W. Daniell, N.-Y. Topsøe and H. Knözinger, *Langmuir*, 2001, **17**, 6233–6239.
62 T. Montanari, E. Finocchio and G. Busca, *J. Phys. Chem. C*, 2011, **115**, 937–943.